



HAL
open science

Post-buckling analysis of elastoplastic sandwich columns by means of an enriched 1D finite element model

Kahina Sad Saoud, Philippe Le Grogneç

► To cite this version:

Kahina Sad Saoud, Philippe Le Grogneç. Post-buckling analysis of elastoplastic sandwich columns by means of an enriched 1D finite element model. *International Journal of Solids and Structures*, 2017, 129, pp.90 - 102. 10.1016/j.ijsolstr.2017.09.009 . hal-01699456

HAL Id: hal-01699456

<https://ensta-bretagne.hal.science/hal-01699456>

Submitted on 17 May 2021

HAL is a multi-disciplinary open access archive for the deposit and dissemination of scientific research documents, whether they are published or not. The documents may come from teaching and research institutions in France or abroad, or from public or private research centers.

L'archive ouverte pluridisciplinaire **HAL**, est destinée au dépôt et à la diffusion de documents scientifiques de niveau recherche, publiés ou non, émanant des établissements d'enseignement et de recherche français ou étrangers, des laboratoires publics ou privés.

Post-buckling analysis of elastoplastic sandwich columns by means of an enriched 1D finite element model

Kahina Sad Saoud^{a,b}, Philippe Le Grogne^{a,c,*}

^a*Mines Douai, Polymers and Composites Technology & Mechanical Engineering Department,
941 rue Charles Bourseul, CS 10838, 59508 Douai Cedex, France*

^b*Institut Pprime (UPR 3346 CNRS – ISAE-ENSMA),
1 avenue Clément Ader, BP 40109, 86961 Chasseneuil-Futuroscope Cedex, France*

^c*ENSTA Bretagne, FRE CNRS 3744, IRDL,
2 rue François Verny, 29806 Brest Cedex 9, France*

Abstract

An advantageous 1D finite element model is designed in the present paper so as to analyze in an efficient way the post-buckling behavior of sandwich beams, known to be commonly responsible for the final collapse of such structures. An enriched beam formulation is defined, where the relatively thin skin layers are modeled as Timoshenko-Reissner beams, as they may undergo large rotations at advanced post-buckled stages. As for the homogeneous core layer, its complex behavior is represented by specific kinematics involving hyperbolic functions. The numerical model is developed within a total Lagrangian formulation framework, considering purely elastic behavior for the skins and an elastoplastic core material. The 1D finite element program incorporates effective incremental control techniques, namely arc-length methods and branch-switching procedures, in order to cope with limit and bifurcation points due to material and geometric non-linearities. A series of incremental calculations is performed in the case of axially compressed columns, exhibiting both global and local buckling modes depending on the geometric and material features. Secondary bifurcations, giving rise to unstable post-buckled solutions, are encountered in most cases due to the operating modal interaction phenomena. The results are compared with reference numerical computations achieved using a 2D finite element customized program.

Keywords: Sandwich structures, Global/local buckling, Elastoplasticity, Modal interaction, Enriched kinematics, Finite element modeling

1. Introduction and scope

Sandwich composites are increasingly involved in various advanced applications from aerospace, marine or transportation industries, owing to their advantageous combined mechanical, electrical, thermal and

*Corresponding author.

Email address: philippe.le_grogne@ensta-bretagne.fr (Philippe Le Grogne)

optical properties, among others. Such materials are classically composed of two thin and stiff metallic or composite skins, separated by a thicker and softer foam core. The resulting structure combines thus both an extreme lightweight due to the low density core material, and strong mechanical properties arising from the skins and their distance to the middle surface of the composite. In spite of all these benefits, sandwich materials suffer from some weaknesses, mostly inherent to their heterogeneous structure. Among them, the buckling phenomenon is known to be one of the major causes for the final collapse of such materials and therefore it has been the subject of numerous studies in the last few decades (see [1] as one of the first leading references in the field). One usually distinguishes two types of geometric instabilities in sandwich structures, namely the global buckling under overall compression and the so-called wrinkling (or local buckling) of the faces, which may appear insofar as they undergo compressive stresses. On one hand, the global buckling of a sandwich material can be easily viewed as the classical buckling of a homogeneous structure as soon as the equivalent properties have been properly derived. On the other hand, the local buckling analysis of sandwiches requires the use of advanced models, since classical buckling solutions for beams or plates are no longer valid.

A significant amount of the existing numerical contributions on sandwich buckling relies on laminated composite displacement-based theories which are formulated on the basis of conventional assumptions for homogeneous beams/plates. In this respect, the most elementary bending models are based upon Euler-Bernoulli/Love-Kirchhoff hypotheses, stating that cross-sections initially perpendicular to the neutral axis/plane of the beam/plate remain straight and normal to the mid-axis/plane after deformation. As the transverse shear deformation effects are not included, these assumptions are no longer valid when dealing with moderately thick structures. In order to overcome this shortcoming, first-order shear deformation theories (FSDT, also referred to as Timoshenko/Reissner-Mindlin theories for beams/plates) have emerged. They maintain that the deformed cross-sections remain plane, but not necessarily perpendicular to the deformed neutral axis/plane (see [2] and [3], for instance). The resulting shear strain distributions are uniform through the thickness (rather than parabolic as practically observed in the case of a homogeneous structure) and thus, shear correction factors are needed so as to assess the transverse shear forces accurately. The determination of these factors is usually not an easy task as it depends on many parameters such as the geometry, loading and boundary conditions (see [4] for further details). Therefore, as an alternative, higher-order shear deformation theories (HSDT) and refined shear deformation theories (RSDT) have been developed, which enable a more realistic description of the shear strain distribution (without any correction), thanks to the introduction of non-linear terms in the displacement fields. The enrichment functions (for the longitudinal/in-plane displacements) may range from polynomials (among many other authors, Ambartsumian [5] and Reddy [6] illustrated the well-known case of third-order kinematics) and trigonometric functions (for instance, ordinary and hyperbolic sine/cosine functions were respectively used in [7] and [8]) to exponential functions (see [9], for example). Besides, it would be worth mentioning that the transverse

deflection is in almost all cases assumed to be constant along the thickness direction.

Dealing with laminated composites, one can distinguish two main approaches, namely the equivalent single-layer (ESL) and layer-wise (LW) theories, according to whether the kinematic fields are described in a global or discrete way. In ESL theories, the displacement field is assumed to be represented by a unique expression across the whole thickness of the composite structure. This may lead to acceptable global stress distributions but completely inappropriate results regarding the interlaminar stresses, and increasing the order of the displacement field is not supposed to fix the problem [10]. For a detailed literature review on the use of ESL theories in the general case of laminated composites, the interested reader may refer to [11] and [12], for instance. In contrast, LW theories rely on piecewise displacement fields, which offer a more realistic representation of the composite through-thickness kinematics. Discrete LW theories assume independent displacement fields within each layer, thus making the number of kinematic variables dependent on the number of layers. The displacement continuity conditions at the interfaces between adjacent layers enable then the total number of degrees of freedom to be reduced [13, 14]. In order to minimize the computational cost of the discrete LW class models, one can resort to the well-known zig-zag theory, as in [15], among many others. In zig-zag models, the in-plane displacements are first defined in a global way (generally using a first-order representation) and then supplemented by piecewise zig-zag functions which ensure the continuity of displacements but also transverse stresses at each interface between successive layers (an overview on zig-zag and refined zig-zag models is available in [16]). Advanced solutions such as those based on Carrera's unified formulation (CUF) or generalized unified formulation (GUF) have emerged recently. Further details on these methods may be found for instance in [17, 18], and benchmark analyses of many theories and models are gathered in the review articles by Ghugal and Shimpi [19], Zhen and Wanji [20] and Hu et al. [21].

The above-mentioned theories have been so far widely applied to investigate the buckling of sandwich structures, which can be viewed as special laminated composites. However, dealing with classical sandwich structures, with typically homogeneous thick and soft core materials compared to the skins, the above model classes are still not appropriate tools for an accurate description of the complex behavior of the core layer, especially when the faces are prone to wrinkle.

Furthermore, the post-critical behavior of sandwich structures was considerably less studied in the literature and the very few contributions concern the axial compression of sandwich columns. Hunt et al. [22] first investigated not only the critical buckling loads and modes but also the non-linear post-buckling response of sandwich structures. They put forward analytical and semi-analytical solutions that emphasized the possible interaction between global (primary) and local (secondary) bifurcation modes. Using a more advanced model, Hunt and Wade [23] also studied this interactive buckling phenomenon and captured the localized pattern of the deformed shape corresponding to the unstable post-buckling response of the sandwich structure. The post-critical behavior is all the more unstable when the primary and secondary bifurcation points are close to each other. The latter results were then extended to the case of orthotropic

core materials [24] and imperfect panels including periodic or localized defects [25]. As for Wadee et al. [26], they analytically solved the buckling and advanced post-buckling response of sandwich structures using two different core bending models based on two different beam theories. The same models were finally used to investigate the interactive buckling phenomenon in a sandwich beam/strut under both compression and bending [27, 28].

In view of the preceding works, the present study aims at developing a new specific beam-like finite element model devoted to the analysis of buckling and advanced post-buckling phenomena in sandwich beam-columns (it can be seen as a generalization of a prior 1D model developed by the authors in the context of elastic linearized buckling [29], taking now into consideration full geometric and material non-linearities). Such a 1D model is supposed to be an efficient numerical tool compared to classical 2D (or 3D) finite element models, where both the skin and core layers are represented as 2D (or 3D) continuous media and discretized using solid elements. In the interest of accuracy, a particular emphasis is given to the through-thickness kinematics. While the skins are typically modeled by Timoshenko beams, the displacement fields in the core layer are defined in accordance with analytical solutions previously derived by the authors in the context of buckling analysis of sandwich beam-columns under various loadings, without presupposing any kinematic assumption [30, 31]. Moreover, the case of an elastoplastic core material is handled in the present analysis. Léotoing et al. [32] already considered this eventuality but, in their numerical study, plasticity only occurs during the post-critical response so that buckling remains elastic. In the present work, plastic buckling is examined in the sense that buckling occurs as the core layer behaves plastically.

The original finite element formulation is implemented in a bespoke program whose main objective is to analyze the global/local buckling of sandwich beam-columns as well as the possible interaction between these modes during the post-buckling range. The 1D model is formulated in the context of finite plasticity within a total Lagrangian framework. The numerical computations are performed in an incremental way, with the help of arc-length methods and branch-switching techniques, so as to trace any equilibrium path (possibly involving snap-through or snap-back phenomena) and bifurcate onto the desired primary or secondary branches (without the use of any kind of imperfection), respectively. The present results only concern the case of compressed sandwich columns, for which several responses are observed, depending on geometric and material parameters. In almost all cases, secondary modes are specifically reached, and the corresponding modal interaction phenomena are therefore demonstrated to be responsible for the final collapse of the sandwich structure. The outcomes are finally compared with reference numerical results, carried out by means of a bespoke 2D finite element program involving the same numerical methods, for validation purposes [31].

2. Theoretical modeling

2.1. Problem definition

This study focuses on classical symmetric sandwich beam-columns (with identical skins). One considers a sandwich beam of length L , thicknesses $2h_s$ and $2h_c$ (for the skin and core layers, respectively) and unit depth (see Fig. 1). The two materials constituting the sandwich structure are assumed to be homogeneous and isotropic, with a linear elastic behavior for the skins and an elastoplastic constitutive law for the core. In the plastic regime, the J_2 flow theory is adopted and the plastic threshold of the core material is defined by the von Mises yield function with a linear isotropic hardening. The outline of this paper is to define a *sandwich beam* model in order to investigate the buckling and post-buckling response of such structures in an efficient way. The advanced post-critical behaviors are of special interest, since they particularly involve multi-scale phenomena. Among the loading conditions giving rise to global or local instabilities, the cases of compression and pure bending have already been solved analytically in [30]. In particular, the analytical modal shapes in the core layer, which were obtained without the use of any kinematic assumption, have shown to be very similar for both loading conditions, and they will thus serve as a basis for the definition of the 1D enriched numerical model.

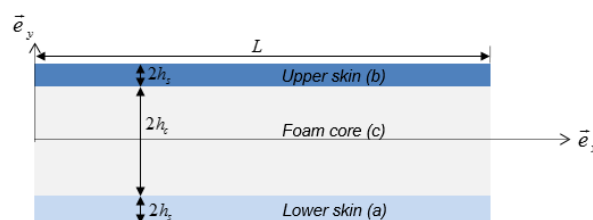


Figure 1: Two-dimensional representation of a sandwich beam-column.

2.2. Kinematics and constitutive laws

The present *sandwich beam* model relies on specific kinematic assumptions for both the skin and core layers, which result in a proper representation of the through-thickness distribution of strain/stress fields, especially when dealing with local instabilities.

2.2.1. Skin layers

For convenience purposes, the skin layers are represented by Timoshenko beams accounting for transverse shear effects. Such a representation makes it possible to deal with all kinds of sandwich beam-columns including short ones, and is more suited for the description of large rotations occurring at advanced post-critical states. Let $(\mathbf{e}_X, \mathbf{e}_Y, \mathbf{e}_Z)$ be a fixed orthonormal basis, where \mathbf{e}_X is the neutral axis of the beam in

hand and \mathbf{e}_Y represents the thickness direction. The displacement field in each face may thus be expressed as follows in the associated coordinate system, according to Timoshenko-Reissner kinematics [33]:

$$\mathbf{U}^i(X, Y) = \begin{cases} U^i(X) - Y \sin(\theta^i(X)) \\ V^i(X) + Y(\cos(\theta^i(X)) - 1) \\ 0 \end{cases} \quad (1)$$

where U^i and V^i are respectively the longitudinal and transverse displacements of the centroid axis of the considered face, and θ^i represents the rotation of its cross-section about the \mathbf{e}_Z axis, Y being the Y -coordinate of a current point relative to its mid-axis (the lower and upper skins are respectively identified with $i = a$ and b).

The Green strain tensor can be therefore written thus:

$$\mathbf{E}^i = \frac{1}{2}(\nabla \mathbf{U}^i + \nabla^T \mathbf{U}^i + \nabla^T \mathbf{U}^i \cdot \nabla \mathbf{U}^i) \quad (2)$$

where the displacement gradient tensor $\nabla \mathbf{U}^i$ takes the following form in the Cartesian basis ($\mathbf{e}_X, \mathbf{e}_Y, \mathbf{e}_Z$):

$$\nabla \mathbf{U}^i = \begin{bmatrix} U_{,X}^i - Y \theta_{,X}^i \cos \theta^i & -\sin \theta^i & 0 \\ V_{,X}^i - Y \theta_{,X}^i \sin \theta^i & \cos \theta^i - 1 & 0 \\ 0 & 0 & 0 \end{bmatrix} \quad (3)$$

Hence, the non-zero strain-displacement relations may be expressed as follows:

$$\begin{cases} E_{XX}^i = U_{,X}^i + \frac{1}{2}(U_{,X}^i{}^2 + V_{,X}^i{}^2) - Y \theta_{,X}^i ((1 + U_{,X}^i) \cos \theta^i + V_{,X}^i \sin \theta^i) + \frac{1}{2} Y^2 \theta_{,X}^i{}^2 \\ 2E_{XY}^i = V_{,X}^i \cos \theta^i - (1 + U_{,X}^i) \sin \theta^i \end{cases} \quad (4)$$

In the general case of an isotropic linear elastic material, the Green strain tensor can be related to the second Piola-Kirchhoff stress tensor Σ^i by the Saint-Venant-Kirchhoff law:

$$\Sigma^i = \mathbf{D}_s : \mathbf{E}^i = \lambda_s \text{tr}(\mathbf{E}^i) \mathbf{I} + 2\mu_s \mathbf{E}^i \quad (5)$$

In Eq. (5), the fourth-order elasticity tensor \mathbf{D}_s (with subscript \bullet_s referring to the skins) is formulated using the Lamé constants λ_s and μ_s , which will be further expressed in terms of the Young's modulus E_s and the Poisson's ratio ν_s as $\lambda_s = \frac{E_s \nu_s}{(1+\nu_s)(1-2\nu_s)}$ and $\mu_s = \frac{E_s}{2(1+\nu_s)}$. Moreover, \mathbf{I} stands for the second-order unit tensor.

Considering here the anti-plane stress state, only the following non-zero stress components will be involved in the subsequent developments:

$$\begin{cases} \Sigma_{XX}^i = E_s E_{XX}^i \\ \Sigma_{XY}^i = 2\mu_s E_{XY}^i \end{cases} \quad (6)$$

2.2.2. Core layer

The complex behavior of the homogeneous foam core is described on the basis of prior analytical and numerical developments by the authors. More precisely, the selected displacement field for the core layer involves modal solutions corresponding to both local and global effects (this issue is discussed in-depth in [29, 30]).

The displacement field within the core layer is finally given by the following expressions:

$$\mathbf{U}^c(X, Y) = \begin{cases} U_0^c(X) + U_1^c(X) \sinh(\frac{\pi}{L}Y) + F(X, Y) \\ V_0^c(X) \cosh(\frac{\pi}{L}Y) + V_1^c(X)Y + G(X, Y) \\ 0 \end{cases} \quad (7)$$

where Y represents the thickness coordinate relative to the mid-axis of the core layer.

The enrichment functions F and G in the previous expressions are intended to describe the local effects that are likely to occur in the core layer. They are thus defined, in accordance with the analytical expressions of the associated buckling modes, as the following combinations of hyperbolic sine and cosine functions:

$$\begin{cases} F(X, Y) = \phi_1(X) \cosh(\alpha Y) + \phi_2(X) \sinh(\alpha Y) + \phi_3(X)Y \cosh(\alpha Y) + \phi_4(X)Y \sinh(\alpha Y) \\ G(X, Y) = \phi_5(X) \cosh(\alpha Y) + \phi_6(X) \sinh(\alpha Y) + \phi_7(X)Y \cosh(\alpha Y) + \phi_8(X)Y \sinh(\alpha Y) \end{cases} \quad (8)$$

It is important to mention that, in the analytical solutions, parameter α only depends on the wavelength $\frac{L}{n}$ of the considered mode (with wavenumber n), which has been shown to remain practically unchanged when varying the geometric and material properties, as far as the first local mode is concerned. Thus, a unique value of this parameter will be retained for all the subsequent examples. The amplitudes $\phi_2(X)$, $\phi_3(X)$, $\phi_5(X)$ and $\phi_8(X)$ are connected to the shape functions associated with the antisymmetric modes and, conversely, $\phi_1(X)$, $\phi_4(X)$, $\phi_6(X)$ and $\phi_7(X)$ are related to the symmetric modes. The contribution of the global mode in Eq. (7) is represented using similar functions where α is replaced by $\frac{\pi}{L}$ (considering $n = 1$ in the analytical expressions). The functions $Y \cosh(\frac{\pi Y}{L})$ and $Y \sinh(\frac{\pi Y}{L})$ are not introduced in this case as they would give rise to singularities due to redundancy. Indeed, since $Y \ll L$, these functions are far too close to the following ones, $\sinh(\frac{\pi Y}{L})$ and $\cosh(\frac{\pi Y}{L})$, respectively. Moreover, it is worth mentioning that the two functions $\sinh(\frac{\pi Y}{L})$ and $\cosh(\frac{\pi Y}{L})$ are almost linear and constant, respectively, within the range considered, so that they can reproduce properly the deformation state of the core layer under bending. Lastly, a constant component $U_0^c(X)$ and a linear one $V_1^c(X)Y$ have been added in the expressions of the longitudinal and transverse displacements, respectively, so as to reproduce also the deformation state under pure compression.

The facings are presumed to be perfectly bounded to the core layer and ad hoc relationships are thus added so as to account for the continuity of the displacements at the top and bottom interfaces:

- at the upper skin/core interface:

$$\mathbf{U}^b(X, -h_s) = \mathbf{U}^c(X, h_c) \implies \begin{cases} U^b + h_s \sin(\theta^b) = U_0^c + U_1^c \sinh(\frac{\pi}{L} h_c) + \phi_1 \cosh(\alpha h_c) + \phi_2 \sinh(\alpha h_c) \\ + \phi_3 h_c \cosh(\alpha h_c) + \phi_4 h_c \sinh(\alpha h_c) \\ V^b - h_s (\cos(\theta^b) - 1) = V_0^c \cosh(\frac{\pi}{L} h_c) + V_1^c h_c + \phi_5 \cosh(\alpha h_c) + \phi_6 \sinh(\alpha h_c) \\ + \phi_7 h_c \cosh(\alpha h_c) + \phi_8 h_c \sinh(\alpha h_c) \end{cases} \quad (9)$$

- at the lower skin/core interface:

$$\mathbf{U}^a(X, h_s) = \mathbf{U}^c(X, -h_c) \implies \begin{cases} U^a - h_s \sin(\theta^a) = U_0^c - U_1^c \sinh(\frac{\pi}{L} h_c) + \phi_1 \cosh(\alpha h_c) - \phi_2 \sinh(\alpha h_c) \\ - \phi_3 h_c \cosh(\alpha h_c) + \phi_4 h_c \sinh(\alpha h_c) \\ V^a + h_s (\cos(\theta^a) - 1) = V_0^c \cosh(\frac{\pi}{L} h_c) - V_1^c h_c + \phi_5 \cosh(\alpha h_c) - \phi_6 \sinh(\alpha h_c) \\ - \phi_7 h_c \cosh(\alpha h_c) + \phi_8 h_c \sinh(\alpha h_c) \end{cases} \quad (10)$$

Taking into consideration the aforementioned displacement continuity constraints, one can rewrite ϕ_1 , ϕ_2 , ϕ_5 and ϕ_6 in terms of the remaining variables as follows:

$$\begin{aligned} \phi_1 &= \frac{1}{\cosh(\alpha h_c)} \left(\frac{1}{2}(U^b + U^a) + \frac{h_s}{2}(\sin(\theta^b) - \sin(\theta^a)) - U_0^c - \phi_4 h_c \sinh(\alpha h_c) \right) \\ \phi_2 &= \frac{1}{\sinh(\alpha h_c)} \left(\frac{1}{2}(U^b - U^a) + \frac{h_s}{2}(\sin(\theta^b) + \sin(\theta^a)) - U_1^c \sinh(\frac{\pi}{L} h_c) - \phi_3 h_c \cosh(\alpha h_c) \right) \\ \phi_5 &= \frac{1}{\cosh(\alpha h_c)} \left(\frac{1}{2}(V^b + V^a) - \frac{h_s}{2}(\cos(\theta^b) - \cos(\theta^a)) - V_0^c \cosh(\frac{\pi}{L} h_c) - \phi_8 h_c \sinh(\alpha h_c) \right) \\ \phi_6 &= \frac{1}{\sinh(\alpha h_c)} \left(\frac{1}{2}(V^b - V^a) - \frac{h_s}{2}(\cos(\theta^b) + \cos(\theta^a) - 2) - V_1^c h_c - \phi_7 h_c \cosh(\alpha h_c) \right) \end{aligned} \quad (11)$$

reducing thus the total number of kinematic unknowns to 14 for the whole sandwich.

Thereby, the in-plane components of the Green strain tensor may be expressed as follows:

$$\begin{cases} E_{XX}^c = \tilde{H}_{XX}^c + \frac{1}{2} \left((\tilde{H}_{XX}^c)^2 + (\tilde{H}_{YY}^c)^2 \right) \\ E_{YY}^c = \tilde{H}_{YY}^c + \frac{1}{2} \left((\tilde{H}_{YY}^c)^2 + (\tilde{H}_{XX}^c)^2 \right) \\ 2E_{XY}^c = \tilde{H}_{XY}^c + \tilde{H}_{YX}^c + \tilde{H}_{XX}^c \tilde{H}_{XY}^c + \tilde{H}_{YY}^c \tilde{H}_{YX}^c \end{cases} \quad (12)$$

where the components of the displacement gradient tensor $\tilde{\mathbf{H}}^c$ are given in Appendix A.

Thereafter, the plane stress hypothesis is adopted. Let us introduce accordingly the generalized strain vector $\boldsymbol{\gamma}_c = \langle E_{XX}^c \ E_{YY}^c \ 2E_{XY}^c \rangle^T$ and stress vector $\mathbf{s}_c = \langle \Sigma_{XX}^c \ \Sigma_{YY}^c \ \Sigma_{XY}^c \rangle^T$.

In the case of an elastic core material, \mathbf{s}_c and $\boldsymbol{\gamma}_c$ are simply related by the following relationship:

$$\mathbf{s}_c = \mathbf{C}_c \boldsymbol{\gamma}_c^e \quad (13)$$

where \mathbf{C}_c refers to the reduced elasticity tensor in plane stress, which may be written as follows in matrix notation:

$$\mathbf{C}_c = \begin{pmatrix} \lambda_c^* + 2\mu_c & \lambda_c^* & 0 \\ \lambda_c^* & \lambda_c^* + 2\mu_c & 0 \\ 0 & 0 & \mu_c \end{pmatrix} \quad (14)$$

with $\lambda_c^* = \frac{2\lambda_c\mu_c}{\lambda_c+2\mu_c}$.

In the case of an elastoplastic core material, use is made of the von Mises yield criterion with a linear isotropic hardening. The classical expression of this criterion in a three-dimensional framework is slightly transformed here so as to fulfill the plane stress condition [34]:

$$f(\mathbf{s}_c, A) = \frac{1}{2}\mathbf{s}_c^T \mathbb{P}\mathbf{s}_c - \frac{1}{3}(\sigma_0^c + A(p))^2 \quad (A = \mathcal{H}_c p) \quad (15)$$

where \mathbb{P} is the deviatoric operator, p is the equivalent plastic strain, and σ_0^c and \mathcal{H}_c stand for the initial yield stress and the (constant) hardening modulus of the core material, respectively.

Following Green and Naghdi [35], the strain vector $\boldsymbol{\gamma}_c$ may be split additively into its elastic and plastic parts:

$$\boldsymbol{\gamma}_c = \boldsymbol{\gamma}_c^e + \boldsymbol{\gamma}_c^p \quad (16)$$

Then, the flow rule is derived from the yield function, according to the generalized standard materials theory:

$$\dot{\boldsymbol{\gamma}}_c^p = \dot{\Lambda} \frac{\partial f}{\partial \mathbf{s}_c} = \dot{\Lambda} \mathbb{P}\mathbf{s}_c \quad (17)$$

where the plastic multiplier $\dot{\Lambda}$ is related to the equivalent plastic strain rate by:

$$\dot{p} = \dot{\Lambda} \sqrt{\frac{2}{3}\mathbf{s}_c^T \mathbb{P}\mathbf{s}_c} \quad (18)$$

3. Finite element implementation

3.1. 1D formulation

The governing equations of the problem are derived from the principle of virtual work within a total Lagrangian framework. The following relation holds for any kinematically admissible displacement variation $\delta\mathbf{U}$:

$$\delta\mathcal{W}_{int}(\delta\mathbf{U}) + \delta\mathcal{W}_{ext}(\delta\mathbf{U}) = 0 \quad (19)$$

On one hand, the virtual work of the internal forces $\delta\mathcal{W}_{int}$ takes the following form:

$$\begin{aligned} \delta\mathcal{W}_{int} &= - \sum_{i=a,b,c} \int_{\Omega_i} \boldsymbol{\Sigma}^i : \delta\mathbf{E}^i dV_i \\ &= - \int_0^L \left(\int_{-h_s}^{h_s} (\Sigma_{XX}^a \delta E_{XX}^a + 2\Sigma_{XY}^a \delta E_{XY}^a) dY + \int_{-h_c}^{h_c} (\Sigma_{XX}^c \delta E_{XX}^c + \Sigma_{YY}^c \delta E_{YY}^c + 2\Sigma_{XY}^c \delta E_{XY}^c) dY \right. \\ &\quad \left. + \int_{-h_s}^{h_s} (\Sigma_{XX}^b \delta E_{XX}^b + 2\Sigma_{XY}^b \delta E_{XY}^b) dY \right) dX \end{aligned} \quad (20)$$

On the other hand, the only applied forces that will be considered in the sequel are localized at the two ends of the sandwich beam-column. The external virtual work $\delta\mathcal{W}_{ext}$ can thus be written as follows:

$$\delta\mathcal{W}_{ext} = \delta\mathbf{q}^T(0)\boldsymbol{\Phi}_0 + \delta\mathbf{q}^T(L)\boldsymbol{\Phi}_L \quad (21)$$

In Eq. (21), \mathbf{q} denotes the following vector of generalized displacements:

$$\mathbf{q}(X) = \langle U^b \ U^a \ U_{,X}^b \ U_{,X}^a \ V^b \ V^a \ V_{,X}^b \ V_{,X}^a \ \theta^b \ \theta^a \ \theta_{,X}^b \ \theta_{,X}^a \ U_1^c \ U_{1,X}^c \ V_0^c \ V_{0,X}^c \ \phi_3 \ \phi_4 \ \phi_7 \ \phi_8 \ \phi_{3,X} \ \phi_{4,X} \ \phi_{7,X} \ \phi_{8,X} \ U_0^c \ U_{0,X}^c \ V_1^c \ V_{1,X}^c \rangle^T \quad (22)$$

where the functions ϕ_1 , ϕ_2 , ϕ_5 , ϕ_6 and their derivatives have been discarded, since they represent auxiliary variables which depend on the key variables (in vector \mathbf{q}) through the continuity conditions (see Appendix A for the corresponding expressions of the derivatives). Φ_0 and Φ_L represent vectors of generalized forces. Since in practice only the facings will be involved with the applied forces, the last 16 components of Φ_0 and Φ_L , associated to the core generalized displacements, will always be zero.

Detailed expressions are given in the sequel for the contribution of both core and skin layers in the internal virtual work (20).

3.1.1. Contribution of the facings

The virtual work of the internal forces acting on the skin layers may be expressed as follows:

$$\begin{aligned} \delta \mathcal{W}_{int}^s &= - \int_0^L \int_{-h_s}^{h_s} (\Sigma_{XX}^a \delta E_{XX}^a + 2\Sigma_{XY}^a \delta E_{XY}^a + \Sigma_{XX}^b \delta E_{XX}^b + 2\Sigma_{XY}^b \delta E_{XY}^b) dY dX \\ &= - \int_0^L \sum_{i=a,b} ((\mathcal{N}_i(1 + U_{,X}^i) - \mathcal{Q}_i \sin \theta^i + \mathcal{M}_i \theta_{,X}^i \cos \theta^i) \delta U_{,X}^i \\ &\quad + (\mathcal{N}_i V_{,X}^i + \mathcal{Q}_i \cos \theta^i + \mathcal{M}_i \theta_{,X}^i \sin \theta^i) \delta V_{,X}^i \\ &\quad - (\mathcal{M}_i((1 + U_{,X}^i) \sin \theta^i - V_{,X}^i \cos \theta^i) + \mathcal{Q}_i((1 + U_{,X}^i) \cos \theta^i + V_{,X}^i \sin \theta^i)) \delta \theta^i \\ &\quad + (\mathcal{M}_i((1 + U_{,X}^i) \cos \theta^i + V_{,X}^i \sin \theta^i) + \mathfrak{M}_i \theta_{,X}^i) \delta \theta_{,X}^i) dX \end{aligned} \quad (23)$$

where \mathcal{N}_i , \mathcal{Q}_i , \mathcal{M}_i and \mathfrak{M}_i are defined by (for a unit depth):

$$\begin{aligned} \mathcal{N}_i &= \int_{-h_s}^{h_s} \Sigma_{XX}^i dY = 2E_s h_s (U_{,X}^i + \frac{1}{2}((U_{,X}^i)^2 + (V_{,X}^i)^2)) + \frac{E_s h_s^3}{3} (\theta_{,X}^i)^2 \\ \mathcal{Q}_i &= \int_{-h_s}^{h_s} \Sigma_{XY}^i dY = 2\kappa \mu_s h_s (-(1 + U_{,X}^i) \sin \theta^i + V_{,X}^i \cos \theta^i) \\ \mathcal{M}_i &= \int_{-h_s}^{h_s} -Y \Sigma_{XX}^i dY = \frac{2E_s h_s^3}{3} ((1 + U_{,X}^i) \cos \theta^i + V_{,X}^i \sin \theta^i) \theta_{,X}^i \\ \mathfrak{M}_i &= \int_{-h_s}^{h_s} Y^2 \Sigma_{XX}^i dY = \frac{2E_s h_s^3}{3} (U_{,X}^i + \frac{1}{2}((U_{,X}^i)^2 + (V_{,X}^i)^2)) + \frac{E_s h_s^5}{5} (\theta_{,X}^i)^2 = \frac{h_s^2}{3} \mathcal{N}_i + \frac{4E_s h_s^5}{45} (\theta_{,X}^i)^2 \end{aligned} \quad (24)$$

with κ standing for the shear correction factor (its value is taken here equal to $\frac{5}{6}$, as for homogeneous beams according to the Timoshenko beam theory).

Hence, Eq. (23) may be rewritten in the following condensed version:

$$\delta\mathcal{W}_{int}^s = - \int_0^L \delta\mathbf{q}^T (\tilde{\mathbf{\Xi}}_b^T \tilde{\mathbf{s}}_b + \tilde{\mathbf{\Xi}}_a^T \tilde{\mathbf{s}}_a + \tilde{\mathbf{b}}_s) dX \quad (25)$$

where $\tilde{\mathbf{\Xi}}_i \in \mathbb{R}^{3 \times 28}$, $\tilde{\mathbf{s}}_i \in \mathbb{R}^3$ and $\tilde{\mathbf{b}}_s \in \mathbb{R}^{28}$. Vectors $\tilde{\mathbf{s}}_i$ are defined by:

$$\tilde{\mathbf{s}}_i = \langle \mathcal{N}_i \ \mathcal{Q}_i \ \mathcal{M}_i \rangle^T \quad (26)$$

The non-zero components of matrices $\tilde{\mathbf{\Xi}}_i$ and vector $\tilde{\mathbf{b}}_s$ are listed in Appendix B.

3.1.2. Contribution of the core

In the core layer, the virtual work of the internal forces writes:

$$\delta\mathcal{W}_{int}^c = - \int_0^L \int_{-h_c}^{h_c} (\Sigma_{XX}^c \delta E_{XX}^c + \Sigma_{YY}^c \delta E_{YY}^c + 2\Sigma_{XY}^c \delta E_{XY}^c) dY dX \quad (27)$$

which may be expressed in the following form:

$$\delta\mathcal{W}_{int}^c = - \int_0^L \int_{-h_c}^{h_c} \delta\mathbf{q}^T (\mathbf{H}_c^T + \mathbf{A}_c^T(\mathbf{q})) \mathbf{s}_c dY dX \quad (28)$$

where $\mathbf{H}_c, \mathbf{A}_c \in \mathbb{R}^{3 \times 28}$.

In Eq. (28), \mathbf{H}_c and \mathbf{A}_c designate respectively the *linear* and *non-linear* parts of $\delta\mathcal{W}_{int}^c$. The non-zero components of \mathbf{H}_c are reported in Appendix B, whereas those of \mathbf{A}_c are not introduced as they are too cumbersome to be presented in this paper.

3.2. Finite element discretization

The problem is now discretized using 3-node isoparametric elements with quadratic shape functions (see Fig. 2).

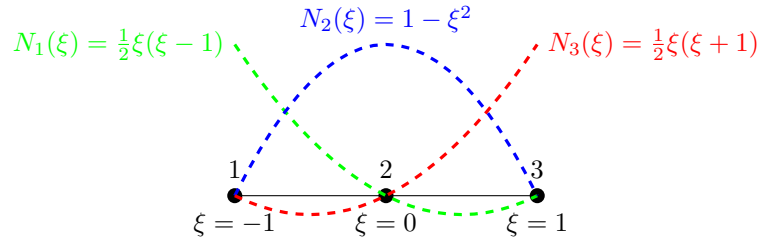


Figure 2: Graphical representation of the interpolation functions of the 3-node reference 1D element.

In view of the kinematic assumptions and continuity conditions, there remain 14 fundamental unknowns which can be brought together in a unique vector $\mathbf{d}(X) = \langle U^b(X) \ U^a(X) \ V^b(X) \ V^a(X) \ \theta^b(X) \ \theta^a(X) \ U_1^c(X) \ V_0^c(X) \ \phi_3(X) \ \phi_4(X) \ \phi_7(X) \ \phi_8(X) \ U_0^c(X) \ V_1^c(X) \rangle^T$.

Within a given finite element e , all the components of vector \mathbf{d} are interpolated in the same way, introducing the elementary nodal displacement vector \mathbf{d}^e composed of the 42 degrees of freedom of the given element and the associated interpolation matrix \mathbf{N} :

$$\mathbf{d} = \mathbf{N}\mathbf{d}^e \quad (29)$$

with $\mathbf{d}^e = \langle \mathbf{d}_1^{eT} \ \mathbf{d}_2^{eT} \ \mathbf{d}_3^{eT} \rangle^T$, where $\mathbf{d}_i^e \triangleq \mathbf{d}(X_i) = \langle U^b \ U^a \ V^b \ V^a \ \theta^b \ \theta^a \ U_1^c \ V_0^c \ \phi_3 \ \phi_4 \ \phi_7 \ \phi_8 \ U_0^c \ V_1^c \rangle_i^T$ contains the 14 degrees of freedom of the i -th node of element e .

Finally, the generalized displacement vector \mathbf{q} may be expressed in terms of \mathbf{d} (by means of a transformation matrix \mathbf{T} including differential operators) and subsequently in terms of \mathbf{d}^e as follows:

$$\mathbf{q} = \mathbf{T}\mathbf{d} = \mathbf{T}\mathbf{N}\mathbf{d}^e \triangleq \mathbf{G}\mathbf{d}^e \quad (30)$$

According to all these definitions, Eq. (19) can be rewritten in the following discretized form:

$$\begin{aligned} \forall \delta \mathbf{d}^e, \quad & \sum_e \int_{-1}^1 \delta \mathbf{d}^{eT} \left(\mathbf{B}_b^T \tilde{\mathbf{s}}_b + \mathbf{B}_a^T \tilde{\mathbf{s}}_a + \mathbf{G}^T \tilde{\mathbf{b}}_s + \int_{-h_c}^{h_c} \mathbf{B}_c^T \mathbf{s}_c \, dY \right) \frac{L_e}{2} d\xi \\ & = \delta \mathbf{d}^T(0) \mathbf{T}^T \Phi_0 + \delta \mathbf{d}^T(L) \mathbf{T}^T \Phi_L \end{aligned} \quad (31)$$

where:

$$\begin{cases} \mathbf{B}_i = \tilde{\mathbf{\Xi}}_i \mathbf{G} & (i = a \text{ or } b) \\ \mathbf{B}_c = \mathbf{B}_L^c + \mathbf{B}_{NL}^c(\mathbf{d}) = (\mathbf{H}_c + \mathbf{A}_c(\mathbf{d})) \mathbf{G} \end{cases} \quad (32)$$

It should be mentioned that the integration with respect to the Y -coordinate has been performed analytically through the thickness of the skins, while a numerical integration using Gaussian quadratures is carried out through the core thickness as it involves more complex hyperbolic functions. Besides, the integration over a real element is replaced by the integration over the reference element, by means of the following variable change: $dX = \frac{L_e}{2} d\xi$ (L_e being the elementary length). A reduced numerical integration scheme (with 2 Gaussian points by element) is employed for the calculation of integrals so as to prevent from any shear-locking problem.

3.3. Solution procedure

The equilibrium equations (31) may be rewritten into the following concise form:

$$\mathbf{R}(\mathbf{U}) = \mathbf{\Psi}(\mathbf{U}) - \mathbf{F} = \mathbf{0} \quad (33)$$

where \mathbf{R} represents the residual vector, $\mathbf{\Psi}$ and \mathbf{F} standing for the global internal and external force vectors, respectively, associated to the global nodal displacement vector \mathbf{U} .

The non-linear equation system (33) is solved using the iterative Newton-Raphson procedure, which requires the computation of the structural tangent stiffness matrix:

$$\mathbf{K}_T = \frac{\partial \mathbf{R}(\mathbf{U})}{\partial \mathbf{U}} = \frac{\partial \mathbf{\Psi}(\mathbf{U})}{\partial \mathbf{U}} \quad (34)$$

The local integration of the state and evolution laws (regarding the core material) is performed using an implicit Euler scheme and the so-called return mapping algorithm, as described in [34]. In particular, the consistent elastoplastic tangent operator, needed for the computation of the tangent stiffness matrix, is evaluated at each iteration n by:

$$\mathbf{C}_c^{ep} = \frac{\partial \mathbf{s}_c}{\partial \gamma_c} = \mathbf{C}_c - \frac{\mathfrak{N}\mathfrak{N}^T}{1 + \beta} \quad (35)$$

where:

$$\begin{aligned} \mathfrak{N} &= \frac{\mathbf{C}_c \mathbb{P} \mathbf{s}_c}{\sqrt{\mathbf{s}_c^T \mathbb{P} \mathbf{C}_c \mathbb{P} \mathbf{s}_c}} \\ \beta &= \frac{2\mathcal{H}_c \mathbf{s}_c^T \mathbb{P} \mathbf{s}_c}{3\mathbf{s}_c^T \mathbb{P} \mathbf{C}_c \mathbb{P} \mathbf{s}_c} \end{aligned} \quad (36)$$

3.3.1. Arc-length method

The nodal displacement vector \mathbf{U} is split into two parts: one denoted by $\tilde{\mathbf{U}}$ contains the unknown degrees of freedom, while the other denoted by $\bar{\mathbf{U}}$ contains the prescribed degrees of freedom. The external force vector and the tangent stiffness matrix are split in a similar way:

$$\mathbf{U} = \begin{Bmatrix} \tilde{\mathbf{U}} \\ \bar{\mathbf{U}} \end{Bmatrix} \quad \mathbf{F} = \begin{Bmatrix} \tilde{\mathbf{F}} \\ \bar{\mathbf{F}} \end{Bmatrix} \quad \mathbf{K}_T = \begin{bmatrix} \tilde{\tilde{\mathbf{K}}}_T & \tilde{\bar{\mathbf{K}}}_T \\ \bar{\tilde{\mathbf{K}}}_T & \bar{\bar{\mathbf{K}}}_T \end{bmatrix} \quad (37)$$

The computer program is developed so as to handle both prescribed loads and prescribed displacements. Either the prescribed displacement or the external load is assumed to be proportional:

$$\begin{aligned} \bar{\mathbf{U}} &= \bar{\mathbf{U}}^0 + \hat{\lambda} \bar{\mathbf{U}}^{ref} \\ \tilde{\mathbf{F}} &= \hat{\lambda} \tilde{\mathbf{F}}^{ref} \end{aligned} \quad (38)$$

where $\hat{\lambda}$ is the control parameter and $\bar{\mathbf{U}}^{ref}$ and $\tilde{\mathbf{F}}^{ref}$ represent reference prescribed quantities (vector $\bar{\mathbf{U}}^0$ related to zero prescribed displacements does not change the *value* of $\bar{\mathbf{U}}$).

A quadratic arc-length method is used in order to proceed on the equilibrium branches in an incremental way (see [36] and [37]). Given a specific arc-length increment Δl , the constraint equation is either of the following relations, depending on whether one has a proportional prescribed displacement or loading:

$$\begin{aligned} \|\Delta \tilde{\mathbf{U}}\|^2 + \Delta \hat{\lambda}^2 \|\bar{\mathbf{U}}^{ref}\|^2 &= \Delta l^2 \\ \|\Delta \tilde{\mathbf{U}}\|^2 + \Delta \hat{\lambda}^2 C_{ref}^2 &= \Delta l^2 \end{aligned} \quad (39)$$

where C_{ref} is a scale parameter which makes the relation consistent dimensionally.

Combining Eq. (39) with the equilibrium equations leads to a quadratic equation in terms of the iterative correction of the control parameter. When solving this quadratic equation, one may encounter severe computational difficulties due to complex roots which occur repeatedly. It is found that an efficient way to cope with these complex roots is to modify the standard solution scheme according to Lam and Morley [38]. The main idea is to project the residual force onto the external load vector. At a current iteration

where complex roots appear, the residual force is split into one component in the load direction and another component orthogonal to this load. This last component is shown to be mainly responsible for the complex roots and should be gradually eliminated.

3.3.2. Branching method

Branch-switching techniques are included in the numerical procedure in order to detect the bifurcation points and bifurcate onto any desired branch. Specific methods are implemented following Riks [36, 39] and Seydel [40]. They are summarized in the four fundamental steps given below:

1. At the end of each increment, it must be checked whether one has gone across one or several critical points. The detection of critical points is based on the singularity of the tangent stiffness matrix, which is factorized following the Crout formula. The critical points are thus determined by counting the number of negative pivots.

2. Each detected critical point has to be isolated in order to determine its nature: limit point or bifurcation point. To do this, the current arc-length Δl is re-estimated several times using a dichotomy-like method. In the case of prescribed loads, a simple way to distinguish a limit point from a bifurcation point is to determine the sign of the *current stiffness parameter* introduced by Bergan et al. [41]:

$$k = \frac{(\tilde{\mathbf{F}}^{ref})^T \tilde{\mathbf{U}}_{Fref}}{(\tilde{\mathbf{U}}_{Fref})^T \tilde{\mathbf{U}}_{Fref}} \quad (40)$$

where $\tilde{\mathbf{U}}_{Fref} = \tilde{\mathbf{K}}_T^{-1} \tilde{\mathbf{F}}^{ref}$. The sign of parameter k changes when passing a limit point, whereas it remains unchanged when passing a bifurcation point. In the case of prescribed displacements, parameter k is computed by:

$$k = -\frac{(\tilde{\mathbf{K}}_T \tilde{\mathbf{U}}^{ref})^T \tilde{\mathbf{U}}_{Uref}}{(\tilde{\mathbf{U}}_{Uref})^T \tilde{\mathbf{U}}_{Uref}} \quad (41)$$

where $\tilde{\mathbf{U}}_{Uref} = -\tilde{\mathbf{K}}_T^{-1} (\tilde{\mathbf{K}}_T \tilde{\mathbf{U}}^{ref})$.

3. If it is a bifurcation point, the step increment is renewed so as to reach a point just behind the bifurcation point.

4. Finally, the switching on a bifurcated branch is performed using the mode injection method [40]: at the first step of a bifurcating branch, the eigenvector $\tilde{\mathbf{Z}}$, solution of $\tilde{\mathbf{K}}_T \tilde{\mathbf{Z}} = \mathbf{0}$, is computed and the following predictions are used:

$$\delta \hat{\lambda} = 0 \quad \delta \tilde{\mathbf{U}} = \pm \frac{\tilde{\mathbf{Z}}}{\|\tilde{\mathbf{Z}}\|} \quad (42)$$

4. Analysis, discussion and validation

Sandwich columns under axial compression show two mode patterns immediately following the buckling onset, mainly depending on the core-to-skin thickness ratio. Indeed, a sufficiently small value of this ratio

promotes the development of a global mode as a first mode (the critical value of this global mode is lower than the one corresponding to the first local mode), whereas a larger value of this ratio firstly gives rise to an antisymmetric/symmetric local mode. In each case, as long as elasticity is concerned, the post-critical behavior is stable and consists in an amplification of the modal deformed shape. For intermediate thickness ratios, the global and minimum local critical values are sufficiently close to each other so that the associated modes may interact during the post-critical stage. This interaction translates in practice into the appearance of a secondary bifurcation right after the primary one on the stable post-critical branch, which corresponds to a local mode if the primary mode is global and vice versa. The secondary post-bifurcated response always reflects an unstable behavior which fatally leads to collapse.

In the following sections, the numerical model presented above is used for the analysis of such post-buckling behaviors. Non-linear computations are performed for various examples involving either an elastic or an elastoplastic core material, so as to cover most of the typical post-buckling responses encountered in the literature. The outcomes are eventually compared with reference numerical results achieved using a 2D finite element program, for validation purposes. Notice that no parametric analysis is performed in the present paper for conciseness purposes. The interested reader may refer to [30] for more details about the influence of geometric and material parameters on the buckling response of sandwich beam-columns.

A few preliminary convergence analyses lead us to adopt the same mesh throughout this study, displaying 100 elements along the column length. Besides, a total number of 12 Gaussian points is retained for the numerical integration through the core thickness in the case of 1D computations. As for the 2D model, 9 eight-node isoparametric quadrangular elements with reduced integration are employed within the core thickness whereas only one element is used in the thickness of each face.

The displacement boundary conditions defined in [30] and depicted in Fig. 3 are here appropriately applied at both ends of the column and no further loading is required.

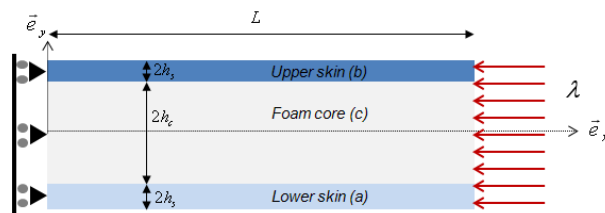


Figure 3: Two-dimensional representation of a sandwich column under axial compression.

At the left end, the longitudinal displacement of both the core and skin layers is prohibited, what corresponds to the following boundary conditions: $U^b(0) = U^a(0) = \theta^b(0) = \theta^a(0) = U_1^c(0) = \phi_3(0) = \phi_4(0) = U_0^c(0) = 0$. Conversely, at the right end, a uniform unit displacement is applied throughout the sandwich thickness in the longitudinal direction, in order to generate compressive stresses in the structure

and induce a buckling phenomenon: $U^b(L) = U^a(L) = U_0^c(L) = -1$ and $\theta^b(L) = \theta^a(L) = U_1^c(L) = \phi_3(L) = \phi_4(L) = 0$. The transverse displacement of an arbitrary point is also fixed so as to prevent the column from rigid modes.

Based upon prior parametric analyses achieved for several geometric and material configurations, parameter α is definitively set at the following value:

$$\alpha = \frac{\pi}{20} \text{ mm}^{-1} \quad (43)$$

4.1. Elastic core material

For the sake of brevity, only two illustrative examples, both involving a modal interaction phenomenon, will be addressed below. The considered geometric and material parameters are summarized in Table 1 (with two possible core thicknesses).

E_s (MPa)	E_c (MPa)	ν_s	ν_c	L (mm)	h_s (mm)	h_c (mm)
50000	70	0.3	0.4	300	0.5	10-30

Table 1: Material and geometric parameters of the elastic sandwich column

4.1.1. Case 1: $h_c = 10 \text{ mm}$

This example is intended to illustrate the interaction between a global primary mode and a local secondary one. The resulting 1D post-buckling response (force-displacement curve identified at the right end of the sandwich column) is depicted in Fig. 4, together with the 2D reference response.

One can readily notice that these equilibrium curves display three distinct parts. The first part is perfectly linear and represents the proportional evolution of the normal force with the enforced displacement during the pre-critical stage. It ends by the occurrence of a primary bifurcation point, which is followed by a plateau. This second part, corresponding to the primary post-bifurcated branch, keeps until the emergence of a secondary bifurcation point. Beyond this point, the third part is characterized by a significant drop of the whole sandwich strength leading to an unstable collapse.

Fig. 5 illustrates successive 1D and 2D deformed shapes (observed at advanced post-critical states after each bifurcation point) that show to be quite similar between each other. Let us mention that all the deformed shapes resulting from the 1D model have been rebuilt into actual 2D shapes as follows: the deformed mid-lines of the upper and lower skins are represented from the $U^b(X)$, $V^b(X)$ and $U^a(X)$, $V^a(X)$ fields, respectively, while the deformed shape of the foam core is plotted as a function of the Y -coordinate by substituting the calculated $U_0^c(X)$, $U_1^c(X)$, $V_0^c(X)$, $V_1^c(X)$, $\phi_1(X)$, $\phi_2(X)$, $\phi_3(X)$, $\phi_4(X)$, $\phi_5(X)$, $\phi_6(X)$, $\phi_7(X)$ and $\phi_8(X)$ fields in Eq. (7).

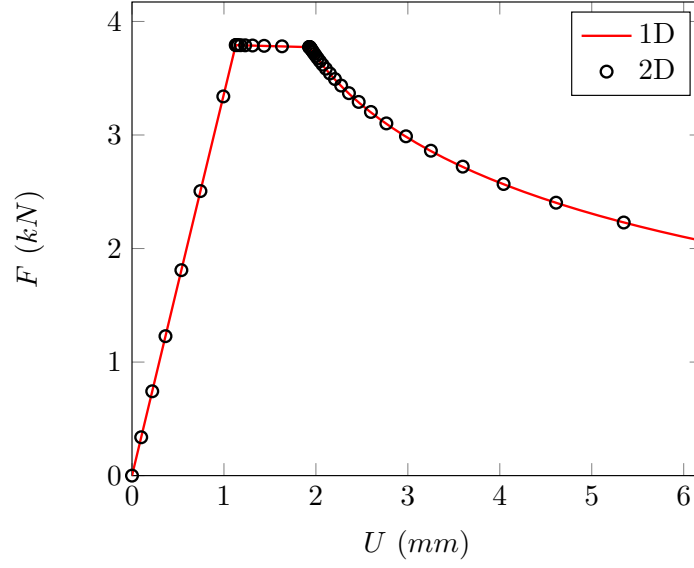


Figure 4: 1D versus 2D force-end shortening response of a sandwich column with an elastic foam core ($h_c/h_s = 20$).

It seems obvious that the sandwich column buckles first in a global mode (Figs. 5(a) and 5(b)). Then, the occurrence of the secondary bifurcation point is marked by the appearance of corrugations starting from the ends of the faces, as shown in Figs. 5(c) and 5(d). Several computations have shown that these geometric localizations were more or less likely to spread along the sandwich column, depending mainly on the thickness ratio h_c/h_s .

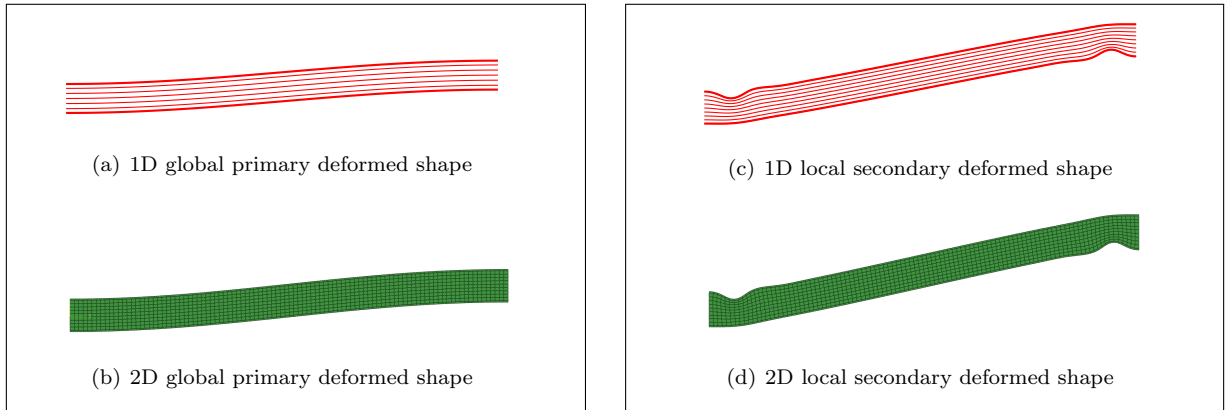


Figure 5: Global-local interaction phenomenon in a sandwich column (magnification factor: $sf=1$).

Let V now be the deflection of the lower skin mid-line at the right end of the column, near the geometric localization. The value of V is plotted against the enforced displacement U in Fig. 6, in both 1D and 2D cases. This feature confirms once more the fair accordance between the two models and therefore the accuracy of the developed 1D model.

Let us finally mention that, with a few adjustments in the boundary conditions and the use of geometric imperfections, this global-local interaction was already discussed in [32] (by the way, the numerical investigations performed by these authors have shown that this problem is very sensitive to the form and size of the initial imperfections). In the present study, the numerical solutions do not depend on any imperfection since the *perfect* equilibrium curves are obtained here.

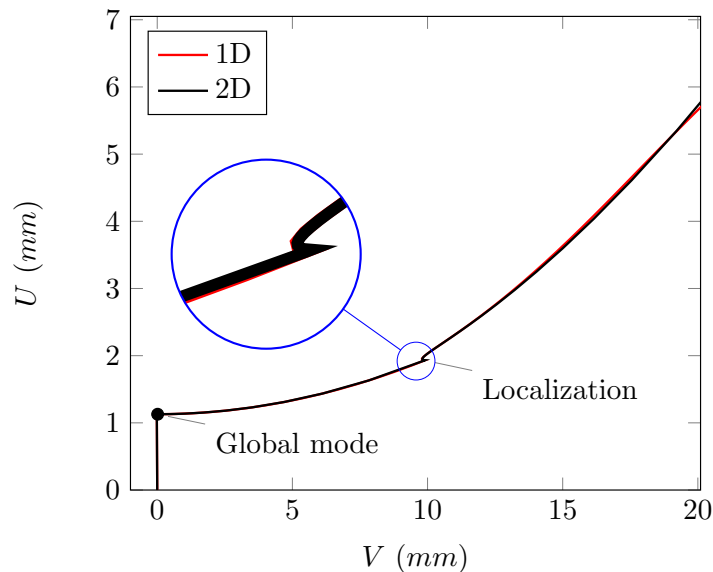


Figure 6: Comparison between 1D and 2D deflections of the lower skin at the right end of the sandwich column with $h_c/h_s = 20$.

4.1.2. Case 2: $h_c = 30$ mm

With a sufficiently thick core layer, the primary buckling mode is expected to be local and the modal interaction, if any, takes place with a global secondary mode. This phenomenon is precisely illustrated in this example. As in the previous case, the post-critical responses depicted in Fig. 7 show also three different parts. One can notice here that, as soon as the first bifurcation point is reached, it is tracked by a second critical point. The primary and secondary critical displacements predicted by the 1D and 2D models are again in good accordance (the relative error does not even reach 2% in the worst case). Nevertheless, it can be seen that, beyond the secondary bifurcation, the two responses take separate post-critical branches.

The 1D and 2D deformed shapes observed after each bifurcation point are shown in Fig. 8. Following the primary bifurcation, it can be observed that the local modes predicted are antisymmetric in both 1D and 2D cases. However, they respectively display 16 and 15 half-waves, as seen in Figs. 8(a) and 8(b) (for comparison purposes, the analytical model by Douville and Le Grogneec [30] provides a local mode with 16 half-waves). This slight difference may potentially explain the disagreement observed in Figs. 8(c) and 8(d). Indeed, crossing the secondary bifurcation point, the two models provide distinct solutions in terms

of deformed shape, yet both of them display a global form: the first one (Fig. 8(c)) can be seen as a global mode obtained with clamped-guided boundary conditions, whereas the last one (Fig. 8(d)) corresponds to the global mode of a simply-supported column.

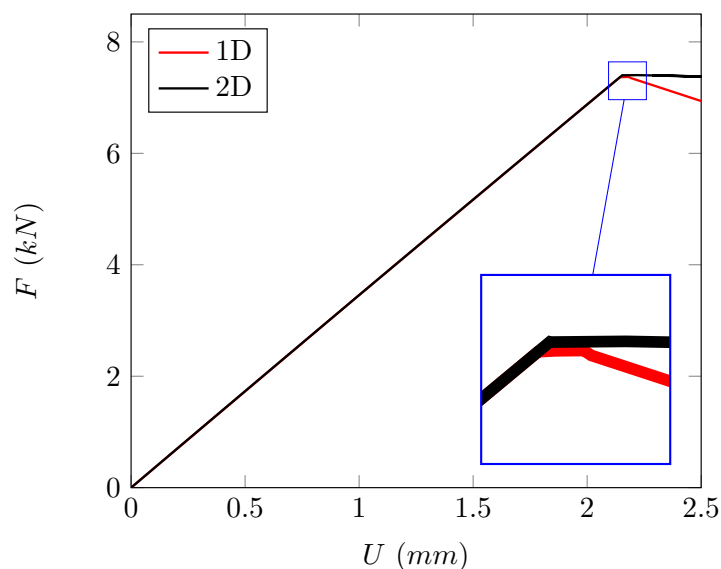


Figure 7: 1D versus 2D force-end shortening response of a sandwich column with an elastic foam core ($h_c/h_s = 60$).

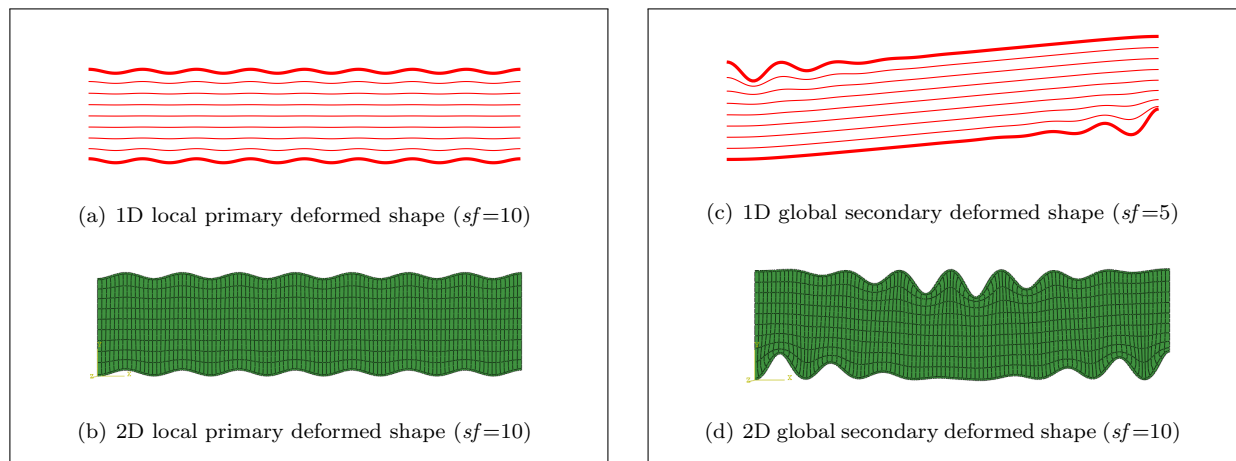


Figure 8: Local-global interaction phenomena in sandwich columns.

Eventually, the resulting primary and secondary critical displacements from both cases 1 and 2 are summarized up in Table 2.

	Numerical model	Primary bifurcation (mm)	Secondary bifurcation (mm)
Case 1	1D	1.128	1.93
	2D	1.128	1.93
Case 2	1D	2.144	2.184
	2D	2.154	2.221

Table 2: Primary and secondary critical displacements of relatively thin and thick elastic sandwich columns

4.2. Elastoplastic core material

As in the elastic case discussed above, two columns with an elastoplastic core material are considered here for illustrative purposes, one with a thick core layer and the other one with a thin core layer. In all the envisaged cases, the yield stress σ_0^c is chosen to be sufficiently small so that buckling occurs in the plastic regime. Other examples, where the buckling phenomenon takes place in the elastic regime and plasticity arises after the primary or secondary bifurcation point, were also treated, but the corresponding results are not presented here since they do not bring anything new. Indeed, in such circumstances, the post-critical response often appears quite similar to those stated above. The most significant difference concerns the unstable secondary behavior, namely the drop of the sandwich strength which is sharper in plasticity.

4.2.1. Case of a relatively thick core layer

The specimen considered in this example has the geometric and material parameters of Table 1, except the core thickness which is taken equal to 35 mm . As in [31], the hardening modulus and the yield stress are $H_c = 50 MPa$ and $\sigma_0^c = 0.28 MPa$, respectively.

Fig. 9 shows the post-critical responses obtained with the 1D and 2D models. In each case, one observes a snap-back behavior, characterized by a turning point which immediately follows the bifurcation point. Though, the 1D response displays a second turning point, which does not appear in the 2D curve.

The deformed shapes depicted in Fig. 10 reveal that the 1D and 2D models give different post-critical solutions, in accordance with Fig. 9. In both cases, the sandwich column buckles first locally, with very close critical displacements (the relative error between the two models is around 3%). The 1D solution displays an antisymmetric mode with 16 half-waves (Fig. 10(a)), whereas the 2D solution gives a symmetric one with 14 half-waves (Fig. 10(b)). Let us recall that, for this example, the analytical solution obtained in [31] predicts an antisymmetric buckling mode with 15 half-waves (the existence of a number of modes having substantially the same critical value justifies the arbitrary nature of the numerical solutions). Thereafter, the buckling mode type (antisymmetric/symmetric) and the associated half-wave number may influence once again the post-critical response and explain the discrepancies between the 1D and 2D results. Hence, the 1D and 2D modal deformed shapes localize in different manners: with the 1D model, the plastic localization

appears at the end of the upper skin (Fig. 10(c)), while it occurs at mid-span and both ends of the sandwich column with the 2D model.

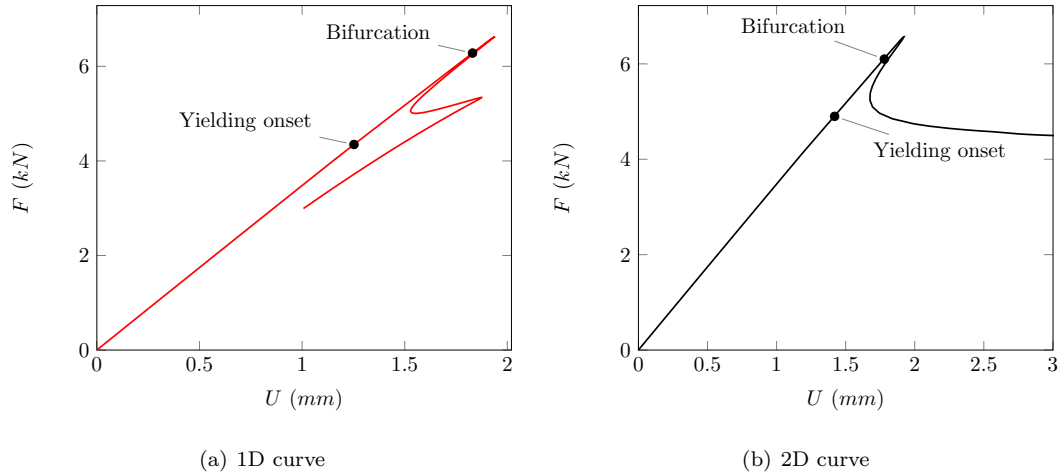


Figure 9: 1D and 2D force-end shortening response of a thick sandwich column with an elastoplastic foam core.

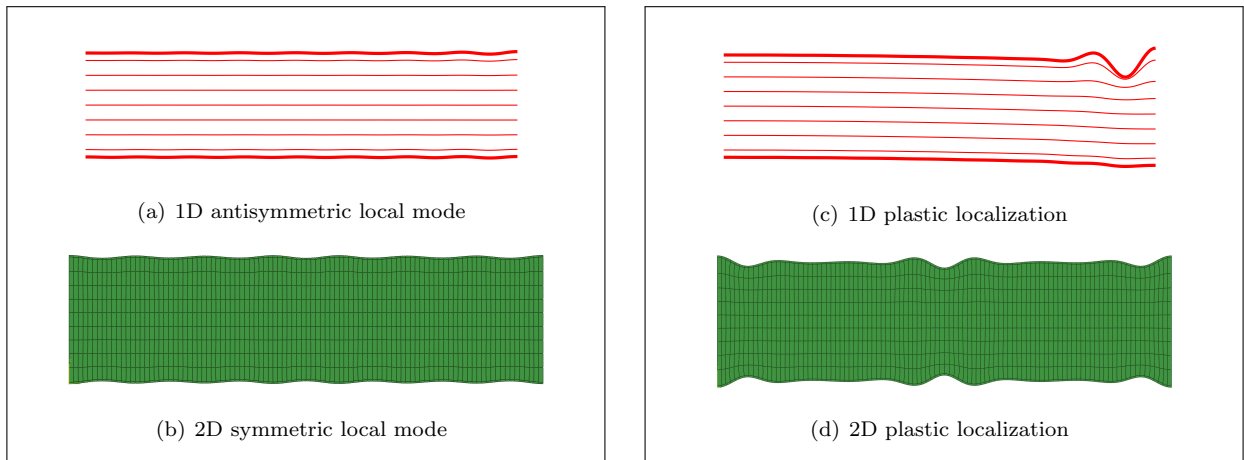


Figure 10: Successive post-critical deformed shapes of a thick elastoplastic sandwich column ($sf=10$).

4.2.2. Case of a relatively thin core layer

Under some particular conditions, the core material may fail in shear due to its low transverse shear strength. This phenomenon, referred to as shear crimping and generally viewed as a global instability, was quite investigated in the last decades and Sullins et al. [42], among other researchers, provided related design rules for axially compressed sandwich structures. Among the very few experimental works investigating the buckling of sandwich beam-columns, Stiftinger and Rammerstorfer [43] particularly observed this failure

mode using specimens made up of high strength aluminum alloy skin layers (elastic) and a crushable foam core material. Next, this special case is illustrated by considering a particular example from [32]. Table 3 provides the corresponding geometric and material properties. Notice that, unlike Léotoing et al. [32], one describes here the shear crimping response of the *perfect* sandwich column, without the use of any kind of imperfection (this extremely unstable behavior is shown again to be highly sensitive to imperfections).

E_s (MPa)	E_c (MPa)	ν_s	ν_c	H_c (MPa)	σ_0^c (MPa)	L (mm)	h_s (mm)	h_c (mm)
70000	175	0.3	0.4	150	1.21	470	0.9	25

Table 3: Material and geometric parameters for the analysis of the shear crimping phenomenon.

The obtained 1D post-critical response is again compared to the 2D one in Fig. 11.

One can readily notice that the two responses are in perfect accordance, both displaying a sharp snap-back. Accordingly, the sandwich column buckles only once, in a global way, and a plastic localization occurs almost immediately after, making the structure unstable and thus leading suddenly to collapse.

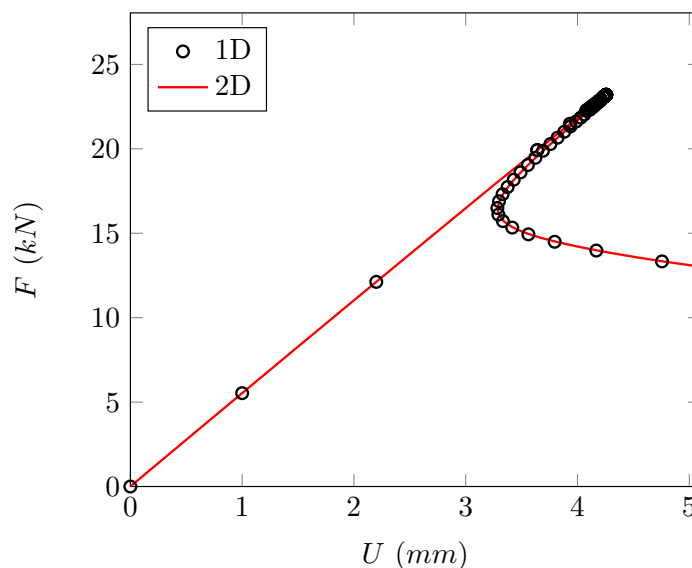


Figure 11: 1D versus 2D force-end shortening response of a sandwich column with an elastoplastic foam core (*shear crimping* behavior).

Fig. 12 illustrates the plastic localization right after its occurrence (Figs. 12(a) and 12(b)) and at an advanced post-critical level (Figs. 12(c) and 12(d)). These deformed shapes show that the localization initially placed at the center of the column slightly extends on both sides during the post-critical advancement. The 1D results are here again in conformity with those of the 2D model.

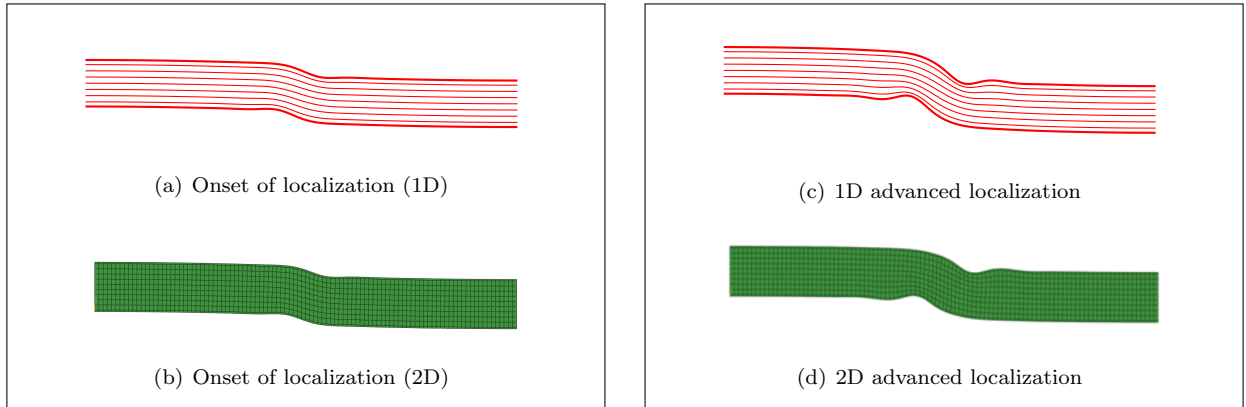


Figure 12: Successive post-critical deformed shapes of a thin elastoplastic sandwich column ($sf=2$).

5. Conclusions

This paper presents a 1D finite element model devoted to the buckling and post-buckling analysis of sandwich beam-columns in an efficient way. In this model, the skins are classically represented by Timoshenko-Reissner beams that may undergo large rotations, whereas special hyperbolic functions are employed so as to describe the displacement profiles along the core thickness. This kinematics is perfectly suited for this issue as it is based on earlier analytical investigations whose results naturally involve such hyperbolic functions in both cases of global and local buckling modes.

The problem is discretized using 3-node Lagrangian 1D elements with 14 degrees of freedom per node. The implemented finite element model includes finite plasticity, arc-length methods and branch-switching procedures so as to deal with the elastic/plastic post-buckling response of sandwich beam-columns up to advanced deformation states. Therefore, such a numerical tool enables one to browse most of the possible post-buckling responses in an efficient way.

Several post-critical behaviors of sandwich columns are particularly investigated here, considering either an elastic or an elastoplastic foam core material. The true elastoplastic equilibrium paths are calculated with a very good accuracy, without resorting to initial imperfections.

- In elasticity, examples presenting secondary bifurcation points are discussed and the underlying modal interaction phenomena are shown to inevitably lead to unstable collapse.
- In plasticity, no secondary bifurcation point is observed but the primary deformed shapes, either local or global, tend to localize, what corresponds in most cases to a sharp snap-back phenomenon.

In all cases, the 1D results are compared with analogous reference 2D computations, performed for validation purposes. The good accordance between these numerical models attests the validity of the designed 1D tool at a substantially reduced computational cost.

Acknowledgments

This research has been supported by the Nord-Pas-de-Calais Regional Council (France), which is gratefully acknowledged.

References

- [1] Allen, H.G., *Analysis and Design of Structural Sandwich Panels* (Pergamon, 1969).
- [2] Timoshenko, S.P., On the correction for shear of the differential equation for transverse vibrations of prismatic bars, *The London, Edinburgh, and Dublin Philosophical Magazine and Journal of Science* **41** (1921) 744–746.
- [3] Reissner, E., The effect of transverse shear deformation on the bending of elastic plates, *Journal of Applied Mechanics* **12** (1945) 69–77.
- [4] Dong, S.B., Alpdogan, C. and Taciroglu, E., Much ado about shear correction factors in Timoshenko beam theory, *International Journal of Solids and Structures* **47** Issue 13 (2010) 1651–1665.
- [5] Ambartsumian, S.A., On the theory of bending plates, *Izv. Otd. Tech. Nauk. AN SSSR* **5** (1958) 69–77.
- [6] Reddy, J.N., A refined non-linear theory of plates with transverse shear deformation, *International Journal of Solids and Structures* **20** Issues 9-10 (1984) 881–896.
- [7] Touratier, M., An efficient standard plate theory, *International Journal of Engineering Science* **29** Issue 8 (1991) 901–916.
- [8] Soldatos, K.P., A transverse shear deformation theory for homogeneous monoclinic plates, *Acta Mechanica* **94** (1992) 195–220.
- [9] Sayyad, A.S., Flexure of thick orthotropic plates by exponential shear deformation theory, *Latin American Journal of Solids and Structures* **10** Issue 3 (2013) 473–490.
- [10] Liu, D. and Li, X., An overall view of laminate theories based on displacement hypothesis, *Journal of Composite Materials* **30** Issue 14 (1996) 1539–1561.
- [11] Reddy, J.N., An evaluation of equivalent-single-layer and layerwise theories of composite laminates, *Composite Structures* **25** Issues 1-4 (1993) 21–35.
- [12] Carrera, E., Theories and finite elements for multilayered, anisotropic, composite plates and shells, *Archives of Computational Methods in Engineering* **9** Issue 2 (2002) 87–140.
- [13] Toledano, A. and Murakami, H., A composite plate theory for arbitrary laminate configurations, *Journal of Applied Mechanics* **54** Issue 1 (1987) 181–189.
- [14] Reddy, J.N. and Robbins, D.H., Theories and computational models for composite laminates, *Applied Mechanics Reviews* **47** Issue 6 (1994) 147–169.
- [15] Di Sciuva, M., A refined transverse shear deformation theory for multilayered anisotropic plates, *Atti della Accademia delle Scienze di Torino* **118** (1984) 279–295.
- [16] Tessler, A., Di Sciuva, M. and Gherlone, M., A consistent refinement of first-order shear deformation theory for laminated composite and sandwich plates using improved zigzag kinematics, *Journal of Mechanics of Materials and Structures* **5** Issue 2 (2010) 341–367.
- [17] Carrera, E., Theories and finite elements for multilayered plates and shells: a unified compact formulation with numerical assessment and benchmarking, *Archives of Computational Methods in Engineering* **10** Issue 3 (2003) 215–296.
- [18] Demasi, L., ∞^6 Mixed plate theories based on the Generalized Unified Formulation. Part II: Layerwise theories, *Composite Structures* **87** Issue 1 (2009) 12–22.
- [19] Ghugal, Y.M. and Shimpi, R.P., A review of refined shear deformation theories of isotropic and anisotropic laminated plates, *Journal of Reinforced Plastics and Composites* **21** Issue 9 (2002) 775–813.

- [20] Zhen, W. and Wanji, C., An assessment of several displacement-based theories for the vibration and stability analysis of laminated composite and sandwich beams, *Composite Structures* **84** Issue 4 (2008) 337–349.
- [21] Hu, H., Belouettar, S., Potier-Ferry, M. and Daya, E.M., Review and assessment of various theories for modeling sandwich composites, *Composite Structures* **84** Issue 3 (2008) 282–292.
- [22] Hunt, G.W., Da Silva L.S. and Manzacchi, G.M.E., Interactive buckling in sandwich structures, *Proceedings of the Royal Society A* **417** (1988) 155–177.
- [23] Hunt, G.W. and Wadee, M.A., Localization and mode interaction in sandwich structures, *Proceedings of the Royal Society A* **454** (1998) 1197–1216.
- [24] Wadee, M.A. and Hunt, G.W., Interactively induced localized buckling in sandwich structures with core orthotropy, *Journal of Applied Mechanics* **65** (1998) 523–528.
- [25] Wadee, M.A., Effects of periodic and localized imperfections on struts on nonlinear foundations and compression sandwich panels, *International Journal of Solids and Structures* **37** Issue 8 (2000) 1191–1209.
- [26] Wadee, M.A., Yiatros, S. and Theofanous, M., Comparative studies of localized buckling in sandwich struts with different core bending models, *International Journal of Non-Linear Mechanics* **45** Issue 2 (2010) 111–120.
- [27] Yiatros, S. and Wadee, M.A., Interactive buckling in sandwich beam-columns, *Journal of Applied Mathematics* **76** Issue 1 (2011) 146–168.
- [28] Yiatros, S., Marangos, O., Wadee, M.A. and Georgiou, C., Localized buckling in sandwich struts with inhomogeneous deformations in both face plates, *Composite Structures* **133** (2015) 630–641.
- [29] Sad Saoud, K. and Le Grogneq, P., An enriched 1D finite element for the buckling analysis of sandwich beam-columns, *Computational Mechanics* **57** Issue 6 (2016) 887–900.
- [30] Douville, M.A. and Le Grogneq, P., Exact analytical solutions for the local and global buckling of sandwich beam-columns under various loadings, *International Journal of Solids and Structures* **50** Issues 16-17 (2013) 2597–2609.
- [31] Le Grogneq, P. and Sad Saoud, K., Elastoplastic buckling and post-buckling analysis of sandwich columns, *International Journal of Non-Linear Mechanics* **72** (2015) 67–79.
- [32] Léotoing, L., Drapier S. and Vautrin, A., Nonlinear interaction of geometrical and material properties in sandwich beam instabilities, *International Journal of Solids and Structures* **39** Issues 13-14 (2002) 3717–3739.
- [33] Reissner, E., On one-dimensional finite-strain beam theory: The plane problem, *Journal of Applied Mathematics and Physics* **23** (1972) 795–804.
- [34] Simo, J.C. and Hughes, T.J.R., *Computational inelasticity* (Springer, 1998).
- [35] Green, A.E. and Naghdi, P.M., A general theory of an elastic-plastic continuum, *Archive for Rational Mechanics and Analysis* **18** (1965) 251–281.
- [36] Riks, E., An incremental approach to the solution of snapping and buckling problems, *International Journal of Solids and Structures* **15** Issue 7 (1979) 529–551.
- [37] Crisfield, M.A., *Non-Linear Finite Element Analysis of Solids and Structures (Volume 1). Essentials* (John Wiley & Sons, 1991).
- [38] Lam, W.F. and Morley, C.T., Arc-length method for passing limit points in structural calculation, *Journal of Structural Engineering* **118** Issue 1 (1992) 169–185.
- [39] Riks, E., On formulations on path-following techniques for structural stability analysis, *New Advances in Computational Structural Mechanics* (Elsevier, 1991) 65–80.
- [40] Seydel, R., *Practical Bifurcation and Stability Analysis. From Equilibrium to Chaos* (Springer-Verlag, 1994).
- [41] Bergan, P.G., Horrigmoe, G., Krakeland, B. and Soreide, B., Solution techniques for non-linear finite element problem, *International Journal for Numerical Methods in Engineering* **12** (1978) 1677–1696.
- [42] Sullins, R.T., Smith, G.W. and Spier, E.E., *Manual for Structural Stability Analysis of Sandwich Plates and Shells* NASA

Contractor Report No. 1457 (National Aeronautics and Space Administration, 1969).

[43] Stiftinger, M.A. and Rammerstorfer, F.G., Face layer wrinkling in sandwich shells – theoretical and experimental investigations, *Thin-Walled Structures* **29** Issues 1-4 (1997) 113–127.

Appendix A. Useful expressions in the core layer

The displacement gradient tensor components in the foam core write:

$$\begin{aligned}
\tilde{H}_{XX}^c &= U_{0,x}^c + U_{1,x}^c \sinh\left(\frac{\pi}{L}Y\right) + \phi_{1,x} \cosh(\alpha Y) + \phi_{2,x} \sinh(\alpha Y) + \phi_{3,x} Y \cosh(\alpha Y) + \phi_{4,x} Y \sinh(\alpha Y) \\
\tilde{H}_{XY}^c &= U_1^c \frac{\pi}{L} \cosh\left(\frac{\pi}{L}Y\right) + \phi_{1,x} \alpha \sinh(\alpha Y) + \phi_{2,x} \alpha \cosh(\alpha Y) + \phi_3 [\cosh(\alpha Y) + Y \alpha \sinh(\alpha Y)] \\
&\quad + \phi_4 [\sinh(\alpha Y) + Y \alpha \cosh(\alpha Y)] \\
\tilde{H}_{YX}^c &= V_{0,x}^c \cosh\left(\frac{\pi}{L}Y\right) + V_{1,x}^c Y + \phi_{5,x} \cosh(\alpha Y) + \phi_{6,x} \sinh(\alpha Y) + \phi_{7,x} Y \cosh(\alpha Y) + \phi_{8,x} Y \sinh(\alpha Y) \\
\tilde{H}_{YY}^c &= V_0^c \frac{\pi}{L} \sinh\left(\frac{\pi}{L}Y\right) + V_1^c + \phi_5 \alpha \sinh(\alpha Y) + \phi_6 \alpha \cosh(\alpha Y) + \phi_7 [\cosh(\alpha Y) + Y \alpha \sinh(\alpha Y)] \\
&\quad + \phi_8 [\sinh(\alpha Y) + Y \alpha \cosh(\alpha Y)]
\end{aligned} \tag{A.1}$$

Taking into account the displacement continuity constraints at the skin/core interfaces, $\phi_{1,x}$, $\phi_{2,x}$, $\phi_{5,x}$ and $\phi_{6,x}$ may be given by the following expressions:

$$\begin{aligned}
\phi_{1,x} &= \frac{1}{\cosh(\alpha h_c)} \left(\frac{1}{2}(U_{,x}^b + U_{,x}^a) + \frac{h_s}{2}(\theta_{,x}^b \cos \theta^b - \theta_{,x}^a \cos \theta^a) - U_{0,x}^c - \phi_{4,x} h_c \sinh(\alpha h_c) \right) \\
\phi_{2,x} &= \frac{1}{\sinh(\alpha h_c)} \left(\frac{1}{2}(U_{,x}^b - U_{,x}^a) + \frac{h_s}{2}(\theta_{,x}^b \cos \theta^b + \theta_{,x}^a \cos \theta^a) - U_{1,x}^c \sinh\left(\frac{\pi}{L}h_c\right) - \phi_{3,x} h_c \cosh(\alpha h_c) \right) \\
\phi_{5,x} &= \frac{1}{\cosh(\alpha h_c)} \left(\frac{1}{2}(V_{,x}^b + V_{,x}^a) + \frac{h_s}{2}(\theta_{,x}^b \sin \theta^b - \theta_{,x}^a \sin \theta^a) - V_{0,x}^c \cosh\left(\frac{\pi}{L}h_c\right) - \phi_{8,x} h_c \sinh(\alpha h_c) \right) \\
\phi_{6,x} &= \frac{1}{\sinh(\alpha h_c)} \left(\frac{1}{2}(V_{,x}^b - V_{,x}^a) + \frac{h_s}{2}(\theta_{,x}^b \sin \theta^b + \theta_{,x}^a \sin \theta^a) - V_{1,x}^c h_c - \phi_{7,x} h_c \cosh(\alpha h_c) \right)
\end{aligned} \tag{A.2}$$

Appendix B. Useful vectors and matrices

Matrices $\tilde{\Xi}_b$ and $\tilde{\Xi}_a$ are defined by the following non-zero components:

$$\begin{aligned}
\tilde{\Xi}_b(1, 3) &= 1 + U_{,x}^b \\
\tilde{\Xi}_b(1, 7) &= V_{,x}^b \\
\tilde{\Xi}_b(1, 11) &= \frac{h_s^2}{3} \theta_{,x}^b \\
\tilde{\Xi}_b(2, 3) &= -\sin \theta^b \\
\tilde{\Xi}_b(2, 7) &= \cos \theta^b \\
\tilde{\Xi}_b(2, 9) &= -(1 + U_{,x}^b) \cos \theta^b - V_{,x}^b \sin \theta^b \\
\tilde{\Xi}_b(3, 3) &= \theta_{,x}^b \cos \theta^b \\
\tilde{\Xi}_b(3, 7) &= \theta_{,x}^b \sin \theta^b \\
\tilde{\Xi}_b(3, 9) &= \theta_{,x}^b (-1 + U_{,x}^b) \sin \theta^b + V_{,x}^b \cos \theta^b
\end{aligned}$$

$$\begin{aligned}
\tilde{\Xi}_b(3, 11) &= (1 + U_{,x}^b) \cos \theta^b + V_{,x}^b \sin \theta^b \\
\tilde{\Xi}_a(1, 4) &= 1 + U_{,x}^a \\
\tilde{\Xi}_a(1, 8) &= V_{,x}^a \\
\tilde{\Xi}_a(1, 12) &= \frac{h_s^2}{3} \theta_{,x}^a \\
\tilde{\Xi}_a(2, 4) &= -\sin \theta^a \\
\tilde{\Xi}_a(2, 8) &= \cos \theta^a \\
\tilde{\Xi}_a(2, 10) &= -(1 + U_{,x}^a) \cos \theta^a - V_{,x}^a \sin \theta^a \\
\tilde{\Xi}_a(3, 4) &= \theta_{,x}^a \cos \theta^a \\
\tilde{\Xi}_a(3, 8) &= \theta_{,x}^a \sin \theta^a \\
\tilde{\Xi}_a(3, 10) &= \theta_{,x}^a (-(1 + U_{,x}^a) \sin \theta^a + V_{,x}^a \cos \theta^a) \\
\tilde{\Xi}_a(3, 12) &= (1 + U_{,x}^a) \cos \theta^a + V_{,x}^a \sin \theta^a
\end{aligned} \tag{B.1}$$

The non-zero components of vector $\tilde{\mathbf{b}}_s$ are given by:

$$\tilde{b}_s(11) = \frac{4E_s h_s^5}{45} (\theta_{,x}^b)^3 \quad \tilde{b}_s(12) = \frac{4E_s h_s^5}{45} (\theta_{,x}^a)^3 \tag{B.2}$$

The non-zero components of matrix \mathbf{H}_c are:

$$\begin{aligned}
H_c(1, 3) &= \frac{\cosh(\alpha Y)}{2 \cosh(\alpha h_c)} + \frac{\sinh(\alpha Y)}{2 \sinh(\alpha h_c)} \\
H_c(1, 4) &= \frac{\cosh(\alpha Y)}{2 \cosh(\alpha h_c)} - \frac{\sinh(\alpha Y)}{2 \sinh(\alpha h_c)} \\
H_c(1, 11) &= \frac{h_s \cosh(\alpha Y)}{2 \cosh(\alpha h_c)} + \frac{h_s \sinh(\alpha Y)}{2 \sinh(\alpha h_c)} \\
H_c(1, 12) &= \frac{h_s \sinh(\alpha Y)}{2 \sinh(\alpha h_c)} - \frac{h_s \cosh(\alpha Y)}{2 \cosh(\alpha h_c)} \\
H_c(1, 14) &= \sinh\left(\frac{\pi}{L} Y\right) - \frac{\sinh(\alpha Y) \sinh\left(\frac{\pi}{L} h_c\right)}{\sinh(\alpha h_c)} \\
H_c(1, 21) &= Y \cosh(\alpha Y) - \frac{h_c \sinh(\alpha Y)}{\tanh(\alpha h_c)} \\
H_c(1, 22) &= Y \sinh(\alpha Y) - h_c \tanh(\alpha h_c) \cosh(\alpha Y) \\
H_c(1, 26) &= 1 - \frac{\cosh(\alpha Y)}{\cosh(\alpha h_c)} \\
H_c(2, 5) &= \frac{\alpha \sinh(\alpha Y)}{2 \cosh(\alpha h_c)} + \frac{\alpha \cosh(\alpha Y)}{2 \sinh(\alpha h_c)} \\
H_c(2, 6) &= \frac{\alpha \sinh(\alpha Y)}{2 \cosh(\alpha h_c)} - \frac{\alpha \cosh(\alpha Y)}{2 \sinh(\alpha h_c)} \\
H_c(2, 15) &= \frac{\pi}{L} \sinh\left(\frac{\pi}{L} Y\right) - \frac{\alpha \sinh(\alpha Y) \cosh\left(\frac{\pi}{L} h_c\right)}{\cosh(\alpha h_c)}
\end{aligned}$$

$$\begin{aligned}
H_c(2, 19) &= \cosh(\alpha Y) + Y \alpha \sinh(\alpha Y) - \frac{h_c \alpha \cosh(\alpha Y)}{\tanh(\alpha h_c)} \\
H_c(2, 20) &= \sinh(\alpha Y) + Y \alpha \cosh(\alpha Y) - h_c \tanh(\alpha h_c) \alpha \sinh(\alpha Y) \\
H_c(2, 27) &= 1 - \frac{h_c \alpha \cosh(\alpha Y)}{\sinh(\alpha h_c)} \\
H_c(3, 1) &= \frac{\alpha \sinh(\alpha Y)}{2 \cosh(\alpha h_c)} + \frac{\alpha \cosh(\alpha Y)}{2 \sinh(\alpha h_c)} \\
H_c(3, 2) &= \frac{\alpha \sinh(\alpha Y)}{2 \cosh(\alpha h_c)} - \frac{\alpha \cosh(\alpha Y)}{2 \sinh(\alpha h_c)} \\
H_c(3, 7) &= \frac{\sinh(\alpha Y)}{2 \sinh(\alpha h_c)} + \frac{\cosh(\alpha Y)}{2 \cosh(\alpha h_c)} \\
H_c(3, 8) &= \frac{\cosh(\alpha Y)}{2 \cosh(\alpha h_c)} - \frac{\sinh(\alpha Y)}{2 \sinh(\alpha h_c)} \\
H_c(3, 9) &= \frac{h_s \alpha \sinh(\alpha Y)}{2 \cosh(\alpha h_c)} + \frac{h_s \alpha \cosh(\alpha Y)}{2 \sinh(\alpha h_c)} \\
H_c(3, 10) &= \frac{h_s \alpha \cosh(\alpha Y)}{2 \sinh(\alpha h_c)} - \frac{h_s \alpha \sinh(\alpha Y)}{2 \cosh(\alpha h_c)} \\
H_c(3, 13) &= \frac{\pi}{L} \cosh\left(\frac{\pi}{L} Y\right) - \frac{\alpha \sinh\left(\frac{\pi}{L} h_c\right) \cosh(\alpha Y)}{\sinh(\alpha h_c)} \\
H_c(3, 16) &= \cosh\left(\frac{\pi}{L} Y\right) - \frac{\cosh\left(\frac{\pi}{L} h_c\right) \cosh(\alpha Y)}{\cosh(\alpha h_c)} \\
H_c(3, 17) &= \cosh(\alpha Y) + Y \alpha \sinh(\alpha Y) - \frac{h_c \alpha \cosh(\alpha Y)}{\tanh(\alpha h_c)} \\
H_c(3, 18) &= \sinh(\alpha Y) + Y \alpha \cosh(\alpha Y) - h_c \alpha \tanh(\alpha h_c) \sinh(\alpha Y) \\
H_c(3, 23) &= Y \cosh(\alpha Y) - \frac{h_c \sinh(\alpha Y)}{\tanh(\alpha h_c)} \\
H_c(3, 24) &= Y \sinh(\alpha Y) - h_c \tanh(\alpha h_c) \cosh(\alpha Y) \\
H_c(3, 25) &= -\frac{\sinh(\alpha Y)}{\cosh(\alpha h_c)} \\
H_c(3, 28) &= Y - \frac{h_c \sinh(\alpha Y)}{\sinh(\alpha h_c)} \tag{B.3}
\end{aligned}$$